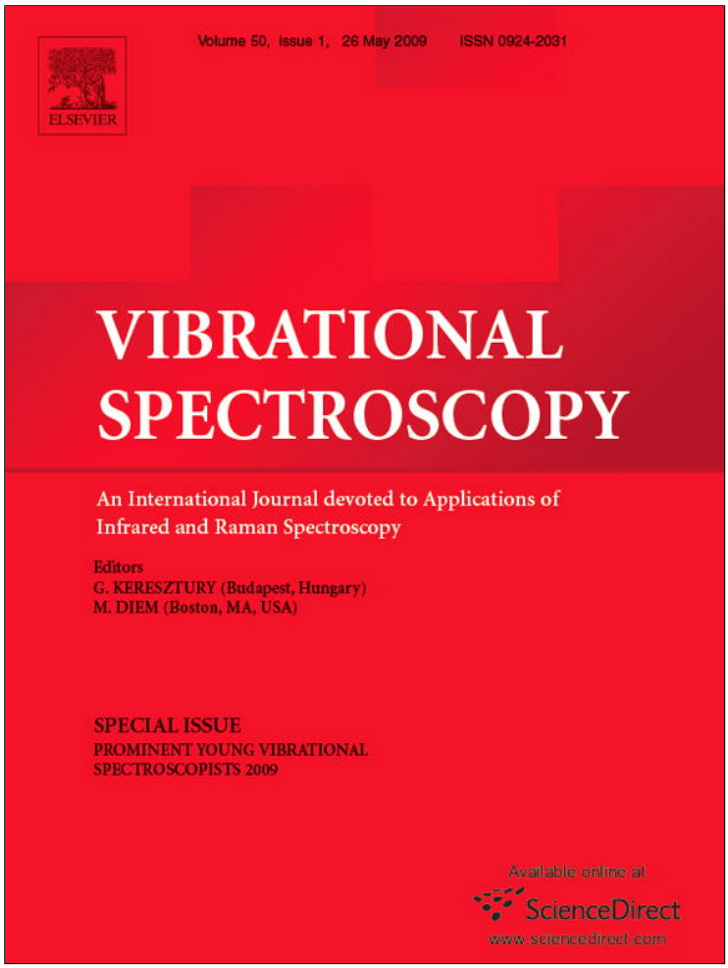

Vibrational Spectroscopy 50 (2009) 36–42

Contents lists available at ScienceDirect

Vibrational Spectroscopy

journal homepage: www.elsevier.com/locate/vibspec

On the vibrations of N_2O trapped in solid *para*-hydrogen

Shui-Ming Hu *, Lei Wan, Jun-He Du, Gang Xu, Wen-Ping Deng, Lei Wu, Shan-Xi Tian, Yang Chen

Hefei National Laboratory for Physical Sciences at the Microscale, University of Science and Technology of China, Jinzhai Road 96, Hefei 230026, China

ARTICLE INFO

Article history:
Received 9 January 2008
Received in revised form 11 July 2008
Accepted 15 July 2008
Available online 26 July 2008

Keywords:
Overtone vibration
Nitrous oxide
Solid molecular hydrogen
Matrix isolation

ABSTRACT

The spectroscopy of molecules trapped in *para*-hydrogen (p-H_2) matrix revealed unique properties of the quantum solid environment. But it has been limited to the low-lying vibrational states while we believe the investigations on the highly excited states may provide new viewpoint of such interesting system. Here we report the infrared spectroscopy of nitrous oxide in solid *para*-hydrogen in the 1000–7000 cm^{-1} region. Fourteen bands including very high overtones like $5\nu_1$ were assigned for each of the three isotopologues of N_2O: $^{14}N_2{}^{16}O$, $^{14}N^{15}N^{16}O$, and $^{15}N^{14}N^{16}O$. All these observed N_2O/p-H_2 bands are found red-shifted. The relative intensity of the $5\nu_1$ band in solid hydrogen matrix was found to be about 100 times higher than that in the gas phase which implies anomalous enhancement by the matrix environment. We also observed "anomalous" high-resolution structures in the ν_3, $\nu_1+\nu_3$ and $2\nu_3$ bands of N_2O/p-H_2. The multiple peaks in the subtle band structures were found regularly separated, temperature-dependent and reversible. The simulation reveals a 142 cm^{-1} high barrier between different orientations of the N_2O molecule in the p-H_2 matrix. The barrier can be accounted for by the hours-long relaxation revealed from the spectra observed at 4.3 K. According to the characters of the observed spectral features, we conclude that the multiple peaks may originate from the multiple orientations of the N_2O molecules isolated in the p-H_2 matrices. It can also interpret that why some bands are with spreading structures while others are just significantly broadened.

1. Introduction

Since the observation of the surprisingly sharp infrared absorption line of solid *para*-hydrogen (p-H_2) in 1989 [1], the solid molecular hydrogen used as matrix host has attracted increasing interests in recent years. Owing to the light mass of H_2 molecule and the "quantum solid" nature of the molecular hydrogen crystal, the spectroscopy of molecules trapped in solid molecular hydrogen (and its isotopes) exhibits some unique characteristics. Tam et al. reported near-free rotation of methane isolated in *para*-hydrogen matrices [2]. The vibrational dephasing of CD_4 molecules in *para*-hydrogen crystals was reported by Katsuki and Momose by observing the temperature dependence of the linewidths of the ro-vibrational transitions [3]. The solid molecular hydrogen matrix has also been successfully applied to trap unstable radicals [4] and ions [5,6]. More examples can be found in the reviews given by Oka [7], Momose and Shida [8] and Anderson and co-workers [9].

To the best of our knowledge, the studies have been limited to the low lying vibrational bands of molecules trapped in *para*-hydrogen matrices. There are very few discussions in the literature on the high overtones and combinational bands. In the present work, we will extend our study to such vibrationally excited states. We hope such measurements can give us a different viewpoint to study such interesting behavior of molecules embedded in quantum solids and can be also used to test the theoretical models. Here we selected the N_2O/p-H_2 system for such purpose.

Nitrous oxide is a very important green house molecule and often used as a reagent in photolysis dynamics studies, the spectroscopy of gas phase nitrous oxide has been extensively studied [10,11]. The matrix isolation spectroscopy have been reported for N_2O in solid N_2[12–14], Ne [15], Ar [14,16–18], Xe [18,19], and in Helium droplet [20]. Lorenz and Anderson reported the ν_3 band of N_2O-$(o$-$D_2)_n$ and N_2O-$(HD)_n$ clusters trapped in solid *para*-hydrogen (p-H_2) matrix [21]. Multiple lines in the ν_3 band of the N_2O/p-H_2 were observed but could not be definitely assigned. Anderson et al. suggested two possible origins of such multiple lines: one is the multiple trapping sites of the N_2O molecule in solid *para*-hydrogen matrix, the other is the N_2O-$(o$-$H_2)_n$ clustering in the matrix.

* Corresponding author. Tel.: +86 551 3606557; fax: +86 551 3602969.
E-mail address: smhu@ustc.edu.cn (S.-M. Hu).

0924-2031/$ – see front matter © 2008 Elsevier B.V. All rights reserved.
doi:10.1016/j.vibspec.2008.07.008

In the present work, the infrared spectra of the N_2O molecules embedded in molecular hydrogen matrices are measured, from the strong fundamental bands to the much weaker overtones extended to the 1.6 μm region. The vibrational assignments are confirmed by a systematic study of different isotopologues of N_2O. The analysis of the subtle structures of the IR spectra observed with high resolution also provides a window to look into the weak interactions between the guest molecule and the p-H_2 matrix.

2. Simulation of N_2O molecule in solid p-H_2 matrix

The equilibrium distance between N_2O and H_2 molecules in the N_2O–H_2 complex is about 3.4 Å [22–24]. This is not far from the spacing between the nearest-neighbor H_2 molecules in the hexagonal close-packed (*hcp*) molecular H_2 crystal (3.8 Å). Meanwhile, the N–N and N–O distances in the N_2O molecule are 1.127 and 1.185 Å, respectively [25]. So it is reasonable to assume that the N_2O molecule will replace a single H_2 position in the matrix. Such structure is illustrated by Fig. 1, which shows the N_2O molecule surrounded by 12 nearest-neighbor p-H_2 molecules. The orientation of the N_2O molecule can be described with the parameters R, α and β. R is the distance from the center of the N_2O molecule to the nearest-neighbor H_2, α is the angle between the x-axis and the projection of the N–N–O molecular axis on the xy plane, and β is the angle from the N–N–O molecular axis to the xy plane.

With the two-body potential of the N_2O–H_2 complex given by Zhou et al. [24], we can estimate the potential energies of one N_2O molecule isolated in the solid hydrogen matrix with different orientations described with R, α and β. For simplicity, only the two-body potential between the N_2O and 12 nearest-neighbor p-H_2 molecules are included in the simulation. All the H_2 molecules are supposed to remain at the $J = 0$ rotational state. When R is equal to the lattice constant of the (*hcp*) molecular H_2 crystal (3.8Å), the potential energy surface with respect to the parameters α and β is as that given in Fig. 2. For symmetry reasons, we only present the surface with α =0–60° and β =0–90°. The whole surface can be extended in the regions $\alpha = -180$ to 180° and $\beta = -90$ to 90°

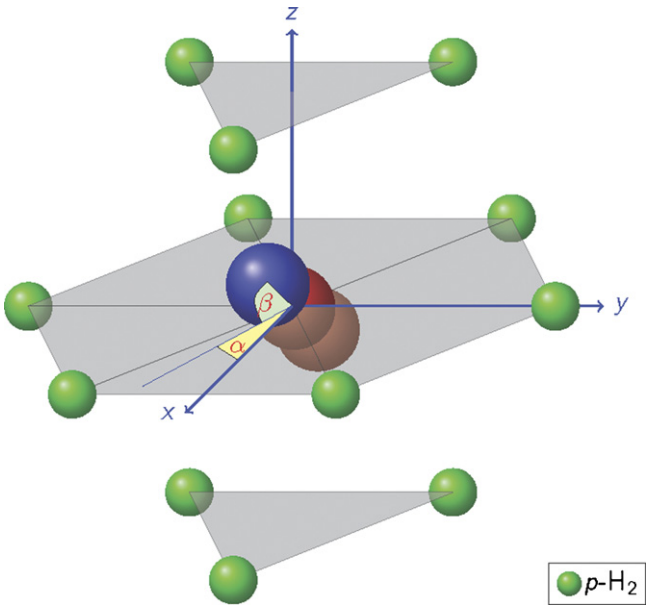

Fig. 1. An N_2O molecule trapped in a *hcp* p-H_2 matrix. Twelve nearest-neighbor surrounding p-H_2 molecules are illustrated. The orientation of the NNO molecule is described with angles α and β. α is the angle between the x-axis and the projection of the N–N–O molecular axis on the xy plane, and β is the angle from the N–N–O molecular axis to the xy plane.

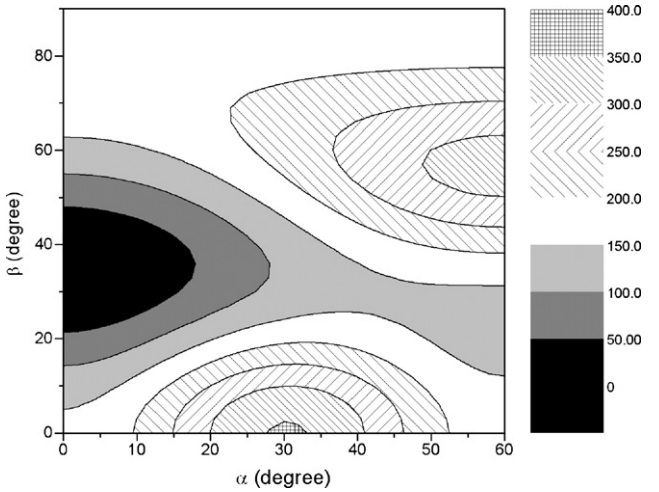

Fig. 2. Potential energy (in cm^{-1}) of N_2O in *hcp* p-H_2 matrix with respect to α and β.

with the formations: $V(-\alpha, \beta) = V(\alpha, \beta)$, $V(\alpha \pm 120°, \beta) = V(\alpha, \beta)$, and $V(\alpha, -\beta) = V(\alpha, \beta)$. According to Fig. 2, there are all together 6 equivalent minima on the potential energy surface, they are at ($\alpha = 0°$ or $\pm 120°$, $\beta = \pm 33°$). A saddle point can be readily found at ($\alpha = 42°$, $\beta = 30°$) with the height of 142 cm^{-1}. This energy is also the barrier height between two nearby minima. Since such barrier is much higher than the rotation energy of a free N_2O molecule (rotational constant $B_0 \simeq 0.4$ cm^{-1}), this means the N_2O molecule will not be able to rotate freely in the molecular hydrogen matrix.

The presence of the N_2O molecule can probably introduce local distortions in the p-H_2 crystal, and the solvation shell can be much larger than what is illustrated in Fig. 1, the real potential energy surface could be more complicated than that shown in Fig. 2, but we can still get some instructive points from such a simulation: (i) there can be quite a few minima on the potential energy surface which are related to different orientations or trapping sites of the N_2O molecule isolated in the solid hydrogen matrix, (ii) the barrier between nearby minima on the potential energy surface can be in the order of one hundred wavenumbers, which is much larger than the rotational energy of a free N_2O molecule and also much larger than the value of $k_BT \simeq 3$ cm^{-1} at $T = 4$ K.

3. Experimental setup

A converter made of a column of $Fe(OH)_3$ catalyst was applied to generate p-H_2. The normal H_2 gas passed through the converter which was maintained at 15–16 K temperature and nearly pure p-H_2 was generated. The purity of the p-H_2 sample was measured by Fourier-transform absorption spectrum near 4150 cm^{-1} of the solid molecular hydrogen. The "impurity" *ortho*-hydrogen (o-H_2) concentration in the prepared sample should be less than 0.1%. It is also confirmed with the Raman spectroscopy of the gas sample by comparing the intensities of the Stokes transitions from *para*-hydrogen ($[v' = 1, J' = 2] \leftarrow [v'' = 0, J'' = 0]$) and from *ortho*-hydrogen ($[v' = 1, J' = 3] \leftarrow [v'' = 0, J'' = 1]$). The details of the Raman measurements can be found in Ref. [26].

Three samples of N_2O were used in the present study, one is natural sample (containing 99% $^{14}N_2{}^{16}O$) bought from Nanjing Special Gas Co., the other two are ^{15}N enriched samples purchased from Icon Services Inc. Concluded from the gas phase infrared spectroscopy and the mass spectroscopy measurements, one ^{15}N enriched sample is with 99% $^{15}N^{14}N^{16}O$ and the other one is with 97% $^{14}N^{15}N^{16}O$. These three samples will be noted as N_2O-446, N_2O-546 and N_2O-456, respectively. The newly prepared p-H_2 gas was mixed with the N_2O sample in a stainless steel bottle and soon

deposited on a BaF_2 substrate. The flow rate was controlled around 1 mmol/min by a mass flow controller. The BaF_2 substrate was attached to the cold head of a closed-cycle cryostat (Janis SHI-4-5). A LakeShore 331S controller was used to control the heating current in a wire attached to the cold head. In this way, the temperature can be adjusted in the range of 3.5–20 K with 0.2 K accuracy. In the measurements, the N_2O/p-H_2 sample was deposited at 4.4 K and then annealed at 5.6 K for 30 min.

The infrared absorption spectra were recorded by a Bruker IFS120HR FT-IR spectrometer. The infrared light beam passed the cold BaF_2 substrate with a 45° incident angle. The entire optical path was evacuated to avoid the atmospheric absorption. The spectra covering the ranges 700–9000 cm^{-1} were recorded with proper selections of the sources (glowbar or tungsten lamp), beam splitters (KBr or CaF_2) and detectors (lN_2 cooled MCT, InSb or Ge). The adopted spectral resolution was 0.02 cm^{-1}.

4. Observed vibrational transitions and assignments

The fundamental bands of N_2O-446, -456 and -546 were observed using low N_2O concentration samples (a few ppm N_2O in p-H_2). While using samples prepared with much higher N_2O concentration (up to 1330 ppm), we were able to observe more overtones and combination bands. The bands of different isotopologues of N_2O can be identified by the comparison of the spectra obtained with different isotopic samples, and the vibrational assignments can be determined by referring to the band centers of N_2O in gas phase [10,11]. Altogether, 14 vibrational bands of N_2O were assigned. All the assignments are given in Table 1. The band shifts with respect to the corresponding gas phase G_v values are presented in the table. The band shift marked with asterisk in the table indicate that the band has a complicated band structure and such bands will be discussed in the next section.

The highest overtone observed in this work is the $5\nu_1$ band. The spectra of the three samples (N_2O-446, -546 and -456) in the $5\nu_1$ band region are shown in Fig. 3. The assignment is based on the following: first, as shown in Fig. 3, we observed nearly the same band structure for the three samples with reasonable band shifts which can be a result of isotopic substitution. Second, according to the gas phase spectrum [10,11], the only observed "bright" states in this region are the (50^00) state and those states have Fermi-resonances with (50^00), like (42^00) and (34^00) states. Actually, the wavefunctions of these states in resonance can be very much mixed, so the vibration quantum numbers used here is rather a simplified notation. The 5 ν_1 band of gas phase $^{14}N_2{}^{16}O$ was found located at 6373.31 cm^{-1}[11], so we assign the band at 6373.16 cm^{-1} shown in Fig. 3(a) to the $5\nu_1$ band of $^{14}N_2{}^{16}O$ in p-H_2. The bands at 6351.30 and 6327.49 cm^{-1} are assigned to the $5\nu_1$ bands of $^{15}N^{14}N^{16}O/p$-H_2 and $^{15}N^{14}N^{16}O/p$-H_2, respectively.

Fig. 4 shows the $n\nu_1$ ($n = 1, 2, 3$ and 5) bands of $^{14}N_2{}^{16}O/p$-H_2. They were recorded using samples with different N_2O/p-H_2 concentrations. We can see the experimental matrix shift varies almost lineally to the quantum number V_1 for $V_1 = 1, 2$ and 3, but the $5\nu_1$ band is not on the trendline shown in Fig. 4. Actually it is surprising that the very high $5\nu_1$ overtone of N_2O can be observed in the solid H_2 matrix if we compare the band intensities in p-H_2 with those in the gas phase. As discussed above, we can assign the $5\nu_1$ band of N_2O in *para*-H_2 with certainty, but we cannot find the $4\nu_1$ band in our measurements for either N_2O-446, -456 or -546. As can be estimated from Fig. 4, the experimental intensity of the $5\nu_1$ band is roughly one fifth of the $3\nu_1$ band of N_2O/p-H_2. As a comparison, according to Refs. [10,11], the gas phase $^{14}N_2{}^{16}O$ $5\nu_1$ band intensity is only 2.6% of the $4\nu_1$, 0.091% of the $3\nu_1$, and 7.7×10^{-4}% of the ν_1 band. It indicates that the very weak $5\nu_1$ band should get enhanced transition strength (over one hundred times) in the p-H_2 matrix than in the gas phase. It presents an interesting example that the matrix environment can enhance some particular transitions. Note that a weak line about several wavenumbers red-shifted to the main line can be found in panels (b)–(e). We assign it to the N_2O clusters since it does not appear in the spectrum with very low N_2O concentration (like in Fig. 4(a)).

Another interesting example is the high bending overtone, $4\nu_2$, this band is evident at 2321.99 cm^{-1} for $^{14}N_2{}^{16}O$, 0.58 cm^{-1} red-

Table 1
Observed vibrational bands of N_2O in p-H_2 matrix, in cm^{-1}

Band [a]	Isotope [b]	G_v [c]	ν_{matrix}	Δ [d]
02^00	456	1144.3334	1143.91	−0.42
	546	1159.9717	1159.90	−0.07
	446	1168.1323	1167.66	−0.47
10^00	456	1280.3541	1279.70	−0.65
	546	1269.8920	1269.36	−0.53
	446	1284.9033	1284.50	−0.40
00^01	556	2154.7259	2152.649	−2.077 [e]
	458	2171.0442	2169.042	−2.002 [e]
	548	2194.0456	2191.978	−2.068 [e]
	547	2197.6486	2195.550	−2.099 [e]
	448	2216.7112	2214.655	−2.056 [e]
	456	2177.6568	2175.592	−2.065 [e]
	546	2201.6053	2199.479	−2.126 [e]
	446	2223.7568	2221.634	−2.123 [e]
04^00	456	2278.1927		
	546	2305.1626	2304.90	−0.26
	446	2322.5731	2321.99	−0.58
12^00	456	2431.3225	2430.16	−1.16
	546	2439.6246	2438.84	−0.78
	446	2461.9964	2460.99	−1.01
20^00	456	2552.4082	2550.88	−1.53
	546	2534.5321	2533.21	−1.32
	446	2563.3394	2561.79	−1.55
01^11	456	2739.5981	2738.95	−0.65
	546	2772.7027	2771.96	−0.74
	446	2798.2926	2797.39	−0.90
02^01	456	3295.4621	3294.10	−1.36
	546	3333.7393	3332.46	−1.28
	446	3363.9780	3362.50	−1.48
10^01	456	3432.1931	3429.356	−2.837 [e]
	546	3443.6500	3440.861	−2.789 [e]
	446	3480.8192	3477.983	−2.836 [e]
22^00	456	3709.8128	3707.89	−1.92
	546	3712.1285	3710.76	−1.37
	446	3748.2518	3746.63	−1.62
30^00	456	3816.4754	3814.10	−2.38
	546	3795.4509	3793.69	−1.76
	446	3836.3710	3834.18	−2.19
00^02	456	4326.6172	4322.58	−4.04 [e]
	546	4373.6061	4369.45	−4.16 [e]
	446	4417.3778	4413.23	−4.15 [e]
20^01	456	4677.7978	4675.37	−2.43
	546	4679.9182	4677.68	−2.24
	446	4730.8250	4728.28	−2.54
50^00	456	n.a.	6327.49	
	546	n.a.	6351.30	
	446	6373.3077	6373.16	−0.15

[a] Quantum numbers of the upper states, $V_1V_2^{\ell_2}V_3$.
[b] Index of different isotopologues of N_2O, 446: $^{14}N^{14}N^{16}O$, 456: $^{14}N^{15}N^{16}O$, 546: $^{15}N^{14}N^{16}O$, 548: $^{15}N^{14}N^{18}O$, 547, $^{15}N^{14}N^{17}O$...
[c] Gas phase values, from Refs. [10,11].
[d] Solid p-H_2 matrix shift, $\Delta = \nu_{matrix} - G_v$.
[e] Band with spreading structure, band origin is indicated with "*" in Fig. 5.

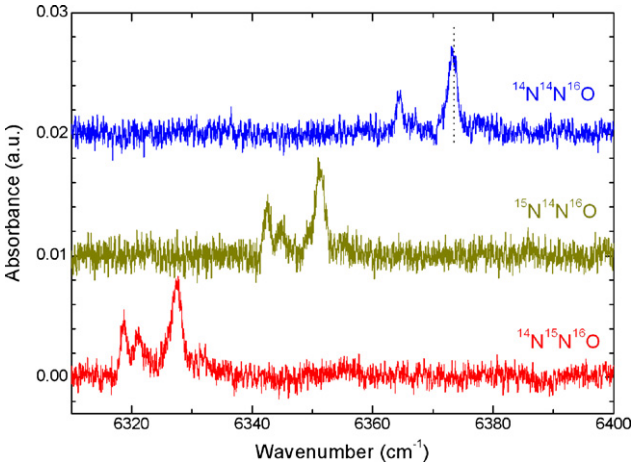

Fig. 3. The $5\nu_1$ band of N_2O/p-H_2. (a) N_2O:p-H_2=1:750, natural N_2O sample, N_2O-446 (99% $^{14}N_2{}^{16}O$). (b) N_2O:p-H_2=1:900, ^{15}N enriched N_2O sample, N_2O-546 (99% $^{15}N^{14}N^{16}O$). (c) N_2O:p-H_2=1:1000, ^{15}N enriched N_2O sample, N_2O-456 (97% $^{14}N^{15}N^{16}O$).

shift to the gas phase band position. But we could not observe the 3 ν_2 band under the same experimental conditions.

It is worth noting that all the observed bands in p-H_2 matrix are red-shifted. The red-shift value of the ν_3 band center in p-H_2 matrix is about 1.6 cm^{-1}, which is considerably large compared with the band shifts of $N_2O(H_2)_n$ clusters observed in a supersonic jet [22,23]. It has been concluded in Refs. [22,23] that the ν_3 band shift of $N_2O(H_2)_n$ varies from blue-shifted to slightly red-shifted when n changes from 1 to 13. The band shift value for the relatively large cluster $N_2O(p\text{-}H_2)_{13}$ is only -0.29 cm^{-1}. If we consider the N_2O doped p-H_2 crystal as a $N_2O(p\text{-}H_2)_n$ cluster with very large n number, it means that adding outer shell p-H_2 molecule will continuously change the energy levels of the cluster. In other words, the large "cluster" can be considered rather soft. In this case, there will be more possible doping sites of the N_2O molecule in the cluster. This consideration coincides with our further investigation on the detailed spectral structure which will be discussed in the next section.

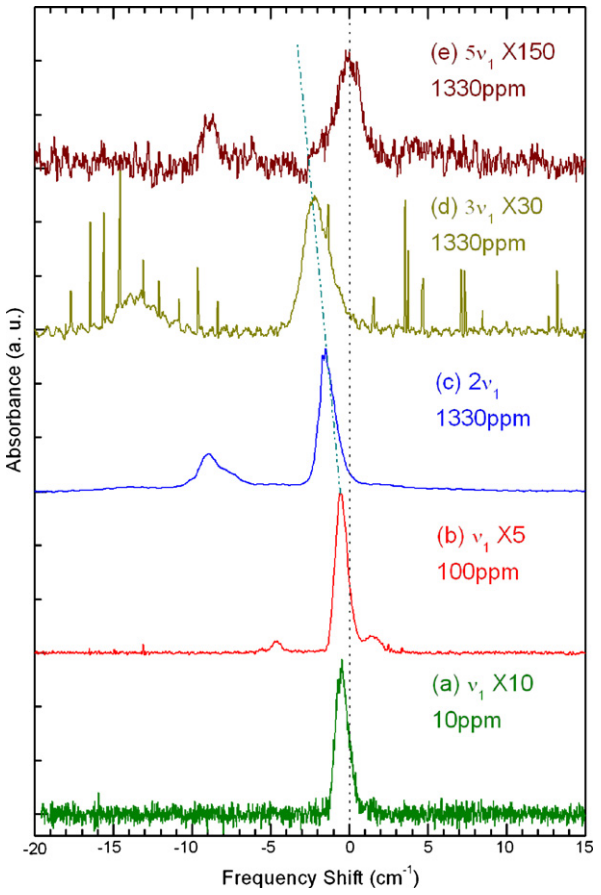

Fig. 4. ν_1 (a and b), $2\nu_1$ (c), $3\nu_1$ (d), and $5\nu_1$ (e) bands of $^{14}N_2{}^{16}O$. (a) 10 ppm N_2O, 49 mmol sample deposited. (b) 100 ppm N_2O, 13 mmol sample deposited. (c) (d) and (e) 1330 ppm N_2O, 80 mmol sample deposited. The frequency shifts in each panel are referred to the respective gas phase G_v values from Ref. [10,11] and given in Table 1. The narrow lines on panel (d) are due to residual water vapor in the optical chamber. The broad line in the lower frequency side of the main peak is assigned to N_2O aggregations (see text).

5. High-resolution subtle band structures

As shown in Fig. 4, most N_2O/p-H_2 bands are broadened with the line widths (FWHM) of about 1 cm^{-1}. We should address that the relatively large line width does not come from instrumental line width, because no structures can be resolved for these bands at a resolution as high as 0.02 cm^{-1}. At the same time, under the same experimental conditions, we have observed resolved spectral structures of the ν_3, $\nu_1+\nu_3$ and $2\nu_3$ bands. These structures are shown in Fig. 5. Note that each of the observed features of these three bands has a beginning line at the lower frequency side. They are 2221.634, 3479.98 and 4413.23 cm^{-1} for ν_3, $\nu_1+\nu_3$ and $2\nu_3$, respectively. These values were denoted as the band origins listed in Table 1. It is very interesting that the weak $2\nu_3$ band looks like the ν_3 band except the frequency scale is doubled: the distance between every two main peaks is 0.72 cm^{-1} in the $2\nu_3$ band instead of 0.36 cm^{-1} in the ν_3 band. The $\nu_1+\nu_3$ band has broadened peaks (FWHM 0.27 cm^{-1}) separated every 0.45 cm^{-1}. Although we will concentrate on the main isotopologue $^{14}N_2{}^{16}O$ in the following discussions, we would address here that we have observed same spectral features for the respective bands of the isotopologues $^{14}N^{15}N^{16}O$ and $^{15}N^{14}N^{16}O$.

The ν_3 band is the strongest one among all the observed vibrational transitions. As shown in Fig. 6, it has a complicated structure spreading in about 2 cm^{-1} range. Fig. 6(a) is the spectrum recorded just after the deposition of about 2 mmol 100 ppm N_2O/

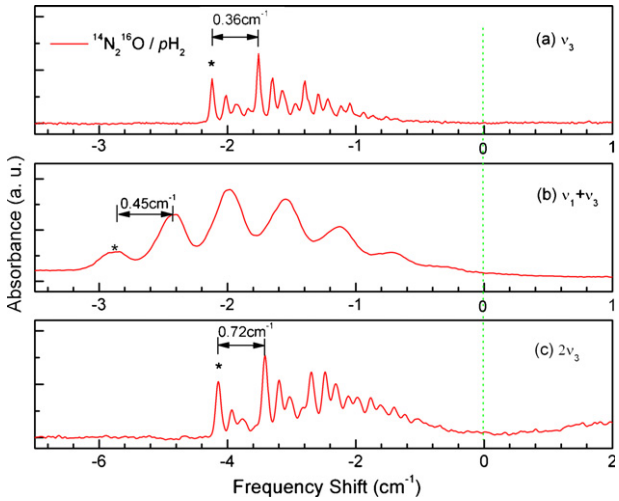

Fig. 5. The ν_3, $\nu_1+\nu_3$ and $2\nu_3$ bands of $^{14}N_2{}^{16}O/p$-H_2. (a) ν_3, (b) $\nu_1+\nu_3$, (c) $2\nu_3$ band. The spectrum was shifted with corresponding gas phase G_v values of each band. The peaks marked with * (the first peak in each band) are noted as band positions used in Table 1. Note the frequency scale of the lowest panel (c) is twice of that in (a) and (b).

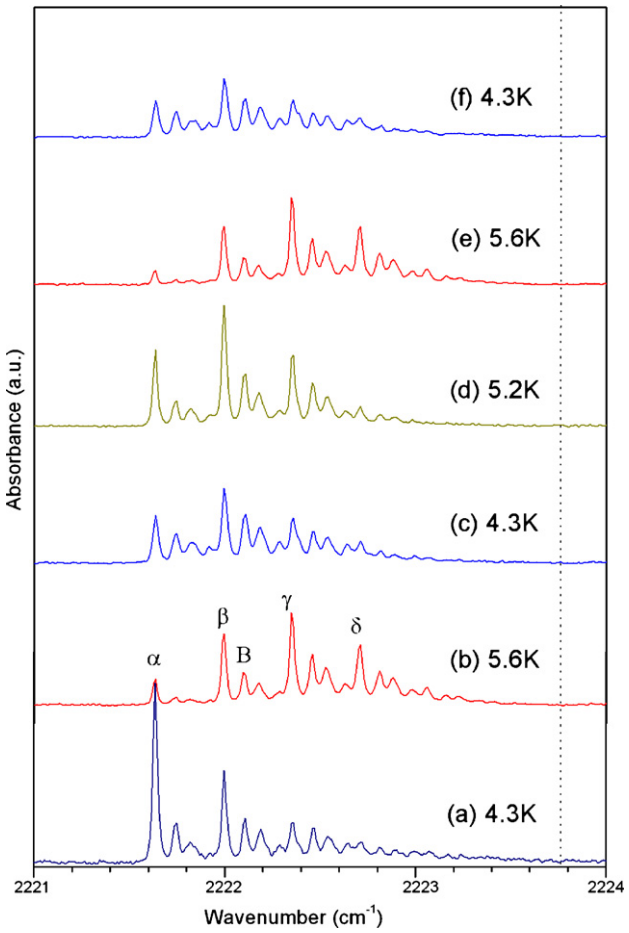

Fig. 6. The ν_3 band of $^{14}N_2{}^{16}O$/*p*-H_2. 100 ppm N_2O-446, 2 mmol sample deposited at 4.4 K. The measurement sequence is (a) → (b) → (c) → (d) → (e) → (f). (a) 4.3 K, recorded just after deposition, (b) 5.6 K, annealing, (c) 4.3 K, after 30 min annealed at 5.6 K, (d) 5.2 K, 3 h after deposition, (e) 5.6 K, 4 h after deposition, (f) 4.3 K, 6 h after deposition. The dotted vertical line on the figure indicates the position of the gas phase band center (2223.757 cm^{-1}).

p-H_2 sample at 4.4 K. Panel (b) is the spectrum recorded during 30 min annealing at 5.6 K. Then the sample was recooled to 4.3 K. It took about 1 h for the spectrum to change from (b) to (c). After that, we carefully warmed up the sample to 5.2 K, and the spectrum shown in (d) was obtained. When the temperature increased to 5.6 K, we got the spectrum (e) which is almost same as that in (b). Then the heating current was cut off and the temperature returned to 4.3 K, the spectrum in (f) was obtained. It is clear that the spectrum in (f) is also same as that in (c) except that the intensities of the corresponding peaks are smaller. This decreasing in absorbance should be a result of H_2 evaporation during the long time measurement.

At least four strong regularly separated peaks can be identified in the spectrum, as marked with α (2221.634 cm^{-1}), β (2221.996 cm^{-1}), γ (2222.353 cm^{-1}) and δ (2222.711 cm^{-1}) in Fig. 6. The separation between two adjacent peaks is 0.36 cm^{-1}. When the temperature increases from 4.3 to 5.6 K, the relative intensities of the peaks γ and δ become higher while the peak α gets lower. There are also some smaller peaks between these main lines. The behavior of these small peaks is similar to those main peaks.

This well *reversible* temperature-dependent feature was also evident in the measurements with much lower N_2O concentration sample (as low as 2 ppm). In a very recent paper, Lorenz and Anderson proposed to assign a few lines of the ν_3 band to the $N_2O(o\text{-}H_2)_n$ clusters in the *p*-H_2 matrix [21]. They assigned the lines at 2221.634 and 2222.086 cm^{-1}("α" and "*B*" lines on our Fig. 6) as the $n = 0$ and $n = 1$ lines, respectively. They suggested to assign other lines in the higher frequency region (like the one at 2221.993 cm^{-1}, "β" line on our Fig. 6) to other trapping sites of N_2O in the *p*-H_2 matrix. Although statistically the quantity of $N_2O(o\text{-}H_2)_n$ in the matrix should be negligible, we still can not exclude the possible contribution to the spectral features from the existence of the $n = 1$ cluster. But because the observed spectral feature is reversible when the temperature changes, we can exclude the possible contribution from larger clusters. The reason is that if there are $N_2O(o\text{-}H_2)_n$ clusters produced continuously due to such "rotational diffusion" proposed in Ref. [27], we can expect that after annealing or when longer time passed, more clusters with larger n will be produced. In other words, this aggregation procedure should be *irreversible*, since we could not expect the aggregated clusters will get broken at the relatively low temperature ($k_BT \sim 3$ cm^{-1}). By the same reason, we can exclude the contribution from aggregated nitrous oxide clusters. We tend to assign the subtle features to the multiple trapping sites (or different orientations) of the N_2O molecule in the *p*-H_2 matrix. This point will be further discussed in the next section.

It is worth noting that the relative intensities of the "β" and "*B*" lines are very different between our measurement and those given in Ref. [21]. This difference may be due to different experimental configurations. In the experimental configuration of Ref. [21], the incident IR beam was parallel to the substrate surface normal, while there was a 45° angle in our case. Since the *c*-axis of the *hcp* molecular hydrogen crystal aligns normal to the substrate surface, the transition dipole with specific direction respect to the crystal axis can give different intensities in these two experimental configurations.

When the temperature changes, we can always observe the intensity redistribution among the peaks in a band. We should address that such intensity redistribution takes very long time (hours) while the temperature of the matrix should get to its equilibrium point within a few minutes or less. This is also a reason that why the subtle structures cannot be rotational structures. As a typical example of such temperature dependence and relaxation behavior, the series spectra of the $\nu_1 + \nu_3$ band are presented in Fig. 7. The spectrum in Fig. 7(a) was obtained just after deposition of about 58 mmol N_2O-446/*p*-H_2(1:1000) sample. Fig. 7(b) was taken during annealing at 5.4 K. After 30 min annealing, the sample was recooled to 4.3 K. Then we recorded the spectrum every 20 min. The spectra recorded at 0.5, 3 and 11 h after the annealing are shown in Figs. 7(c)–(e). We can clearly see the redistribution of the peak intensities during this process. When the temperature decreases, the weight center of the band moves to the lower frequency region. By fitting the spectrum with multiple Gaussian peaks, as shown in Fig. 8, we can get the intensities of respective peaks in each spectrum. The peak positions and the distances between nearby peaks are presented in Table 2. For the two peaks at 3478.88 and 3480.14 cm^{-1}(marked by vertical dash lines in Fig. 7), the intensity values against the time after annealing are depicted in Fig. 9. The relaxation time is about 5 h which can be deduced from an exponential decay curve fitting which is shown in the same figure.

The $2\nu_2 + \nu_3$ band which was observed in the same measurement is also shown in the left part of Fig. 7. In contrast to the $\nu_1 + \nu_3$ band, no high-resolution structures was observed for the $2\nu_2 + \nu_3$ band. But the intensity redistribution phenomenon is also evident here. As a result, the center of the band changes about 0.7 cm^{-1} from (b) to (e).

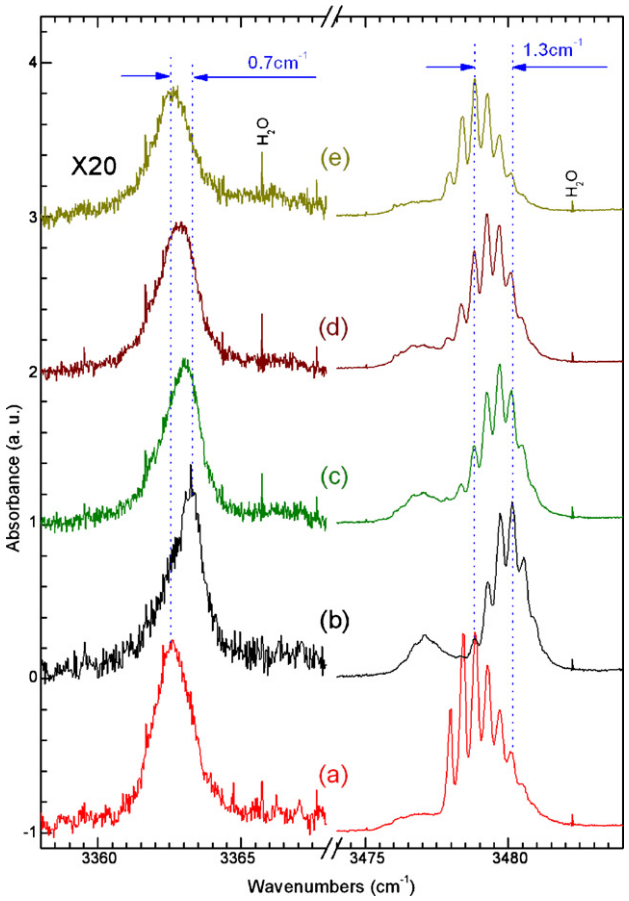

Fig. 7. $2\nu_2 + \nu_3$ and $\nu_1 + \nu_3$ bands of $^{14}N_2{}^{16}O/p\text{-}H_2$. 1000 ppm N_2O-446, 58 mmol sample deposited at 4.4 K. The left part of the spectrum (showing the $2\nu_2 + \nu_3$ band) was multiplied by a factor 20 for better illustration. (a) 4.3 K, recorded just after deposition, (b) 5.4 K, annealing for 30 min, (c) 4.3 K, 0.5 h after annealing, (d) 4.3 K, 3 h after annealing, (e) 4.3 K, 11 h after annealing. The sharp lines are due to residual water vapor in the optical chamber.

Table 2
Peaks of the $\nu_1 + \nu_3$ band of N_2O in p-H_2 matrix, in cm^{-1}

	$^{14}N^{15}N^{16}O$	$^{15}N^{14}N^{16}O$	$^{14}N^{14}N^{16}O$
1	3429.356	3440.861	3477.983
2	3429.799, 0.443	3441.303, 0.442	3478.442, 0.459
3	3430.225, 0.426	3441.741, 0.438	3478.878, 0.436
4	3430.643, 0.418	3442.161, 0.420	3479.305, 0.427
5	3431.060, 0.417	3442.581, 0.420	3479.718, 0.413
6	3431.478, 0.418	3442.989, 0.408	3480.141, 0.423
7	3431.894, 0.416	3443.409, 0.420	3480.554, 0.413
8	3432.273, 0.379		3480.948, 0.394

6. Discussion

As we have discussed above, the characteristics of the subtle features of the vibrational bands of $N_2O/p\text{-}H_2$ allow us to assign them to the transitions of the multiple orientations of N_2O in the p-H_2 matrix. If the energy differences between these orientations are comparable with or smaller than the k_BT value, there will be several most probable orientations during the deposition and annealing. When the temperature changes, there will be a "redistribution" among these orientations, but such "redistribution" may take quite a long time. If we suppose there is an energy barrier when the N_2O molecule defuses from one orientation to another, the relaxation time could be estimated by a simple "tunneling" model: as shown in Section 2, there is a barrier $V_0 = 142\ cm^{-1}$ between two nearby minima ($\alpha = 0°$, $\beta = 33°$) and ($\alpha = 120°$, $\beta = 33°$). For simplicity, suppose it is a rectangular potential with barrier width of $d = \pi/3$, which is half of the distance ($\Delta\alpha$) between these two minima. The N_2O molecule moves as a one dimensional rotor with an effective rotational constant $B' = B_0/\cos^2 33° \simeq 0.57\ cm^{-1}$, and with a rotational energy of $E = k_BT$ which is 3 cm^{-1} at 4.3 K. Then the tunneling probability is $P \approx ((16E(V_0 - E))/V_0^2)\exp(-2d\sqrt{(V_0 - E)/B'}) = 1.5 \times 10^{-15}$. The tunneling rate will be $k = Pf$, and the frequency f can be estimated as $f \simeq E/h = 0.9 \times 10^{11}\ s^{-1}$ where h is the Planck constant. Finally the relaxation time will be $\tau = 1/k = 7 \times 10^3$ s, which coincides in magnitude with our experimental value (5 h).

If the energy differences between the different trapping sites of N_2O are considerably small, or nearly degenerate as shown by our

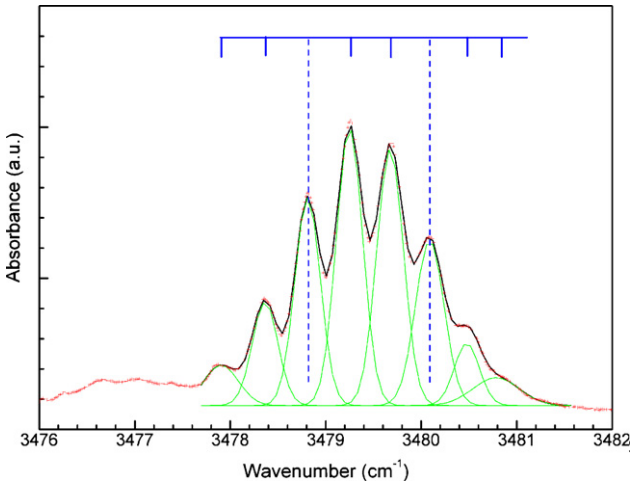

Fig. 8. Multi-peak fitting of the spectrum of the $\nu_1 + \nu_3$ band of $^{14}N_2{}^{16}O/p\text{-}H_2$ obtained 3 h after annealing (Fig. 7(d)). The discrete points show the experimental spectrum and the solid black line shows the fitting result. The widths of the Gaussian peaks (except the two at both sides) are fixed at 0.27 cm^{-1} in the least-squares fitting.

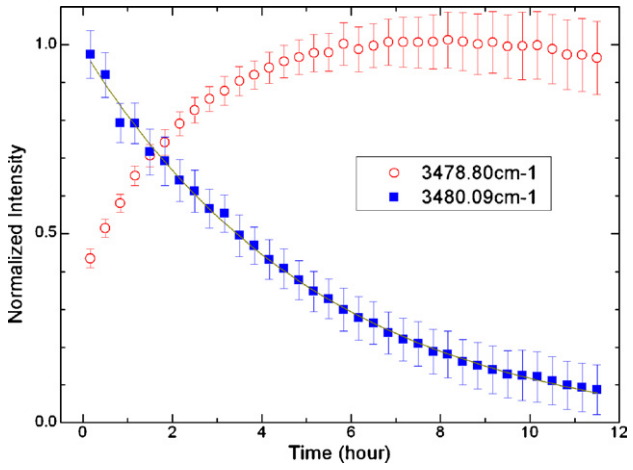

Fig. 9. The relaxation of the $\nu_1 + \nu_3$ band of $^{14}N_2{}^{16}O/p\text{-}H_2$ after annealing: the integrated absorbances (normalized) of the two peaks at 3478.88 and 3480.14 cm^{-1}. These two lines are also indicated with vertical lines in Figs. 7 and 8. Experimental conditions are given in Fig. 7 and in the text. The intensity values were retrieved from the multi-peak fitting of the spectrum. An example of such fitting is given in Fig. 8.

simplified simulation in Section 2, it will be likely that different vibrational states of the doped N_2O molecule can produce different subtle energy structures. In this case, the spectral pattern will be different from band to band. For those vibrational states with large splits between different orientations, there will be isolated sharp peaks as in the cases of the ν_3 and $2\nu_3$ bands. For those vibrational states with small splits, the peaks may overlap, so there will be only broadened features but still with temperature-dependent band centers, as in the case of the $2\nu_2 + \nu_3$ band. This can be a tentative interpretation of the various structures of the vibrational transitions observed in the present work. There will be possibility to calculate the potential energy of a N_2O molecule in bulk hydrogen, but the potential surface can be more complicated: not only the nearest-neighbor H_2 molecules, but also those in the outer shell, can contribute to the interactions. This effect can be found from the fact that the ν_3 band shift observed in the p-H_2 matrix is still very far from that of the free $N_2O(H_2)_n$ clusters with n up to 13 observed in supersonic jet experiment [23]. The full understanding of the spectrum may rely on high-level calculations on very large $N_2O(p\text{-}H_2)_n$ clusters including the consideration of highly excited vibrational modes of N_2O, which may provide some insight of such system but is beyond the feasibility of the present work.

Acknowledgements

The authors are indebted to Dr. M.C. Chan in CUHK for discussions and help in the early stage of this work. S.L. Liu is acknowledged for Raman measurements. D.Q. Xie and J.L. Yang are acknowledged for helpful discussions. This work was jointly supported by the Ministry of Science and Technology of China (2006CB922001, 2007CB815203), the National Natural Science Foundation of China (10728408, 20533060), and the Chinese Academy of Sciences.

References

[1] M. Okumura, M.-C. Chan, T. Oka, Phys. Rev. Lett. 62 (1989) 32.
[2] S. Tam, M.E. Fajardo, H. Katsuki, H. Hoshina, T. Wakabayashi, T. Momose, J. Chem. Phys. 111 (1999) 4191–4198.
[3] H. Katsuki, T. Momose, Phys. Rev. Lett. 84 (2000) 3286–3289.
[4] M. Fushitani, N. Sogoshi, T. Wakabayashi, T. Momose, T. Shida, J. Chem. Phys. 109 (1998) 6346–6350.
[5] M.-C. Chan, M. Okumura, T. Oka, J. Phys. Chem. A 104 (2000) 3775–3779.
[6] X.-F. Wang, L. Andrews, J. Phys. Chem. A 108 (2000) 1103–1106.
[7] T. Oka, Annu. Rev. Phys. Chem. 44 (1993) 299–333.
[8] T. Momose, T. Shida, Bull. Chem. Soc. Jpn. 71 (1998) 1–15.
[9] K. Yoshioka, P.L. Raston, D.T. Anderson, Int. Rev. Phys. Chem. 25 (2006) 469–496.
[10] R.A. Toth, Appl. Opt. 30 (1991) 5289–5315.
[11] R.A. Toth, J. Mol. Spectrosc. 197 (1999) 158–187.
[12] M. Bahou, L. Schriver-Mazzuoli, C. Camy-Peyret, A. Schriver, J. Chem. Phys. 108 (1998) 6884–6891.
[13] A. Łapiński, J. Spanget-Larsen, J. Waluk, J.G. Radziszewski, J. Chem. Phys. 115 (2001) 1757–1764.
[14] L.M. Nxumalo, T.A. Ford, J. Mol. Struct. 327 (1994) 145–159.
[15] L. Wan, G. Xu, L. Wu, Y. Chen, S.-M. Hu, J. Mol. Spectrosc. 249 (2008) 65–67.
[16] H. Chabbi, P.R. Dahoo, B. Gauthier-Roy, A.-M. Vasserot, L. Abouaf-Marguin, J. Phys. Chem. A 104 (2000) 1670–1673.
[17] S. Kudoh, K. Onoda, M. Takayanagi, M. Nakata, J. Mol. Struct. 524 (2000) 61–68.
[18] W.G. Lawrence, V.A. Apkarian, J. Chem. Phys. 97 (1992) 2224–2228.
[19] H. Krueger, E. Weitz, J. Chem. Phys. 96 (1992) 2846–2855.
[20] K. Nauta, R.E. Miller, J. Chem. Phys. 115 (2001) 10254–10260.
[21] B.D. Lorenz, D.T. Anderson, J. Chem. Phys. 126 (2007) 184506.
[22] J. Tang, A.R.W. McKellar, J. Chem. Phys. 117 (2002) 8308.
[23] J. Tang, A.R.W. McKellar, J. Chem. Phys. 123 (2005) 114314.
[24] Y.-Z. Zhou, H. Ran, D.-Q. Xie, J. Chem. Phys. 125 (2006) 174310.
[25] J.-L. Teffo, A. Chédin, J. Mol. Spectrosc. 135 (1989) 389.
[26] Y.-Q. Yu, K. Lin, X.-G. Zhou, H. Wang, S.-L. Liu, X.-X. Ma, J. Phys. Chem. C 111 (2007) 8971–8978.
[27] K. Yoshioka, D.T. Anderson, J. Chem. Phys. 119 (2003) 4731–4742.